Ionization Bands and Electron Affinities of Mixed Boron–Nitrogen BnNn Clusters (n = 3,4,5)

ARTICLE · JANUARY 2006

CITATIONS
13

READS
4

4 AUTHORS, INCLUDING:

Michael S Deleuze
Hasselt University
132 PUBLICATIONS **2,673** CITATIONS

SEE PROFILE

Ionization Bands and Electron Affinities of Mixed Boron−Nitrogen B_nN_n Clusters ($n = 3,4,5$)

M. S. Deleuze,* M. G. Giuffreda, and J.-P. François

Instituut voor MateriaalOnderzoek (IMO), Departement SBG, Limburgs Universitair Centrum, Universitaire Campus, B-3590 Diepenbeek, Belgium

L. S. Cederbaum

Lehrstuhl für Theoretische Chemie, Institut für Physikalische Chemie, Universität Heidelberg, D69120 Heidelberg, Germany

Received: September 13, 1999; In Final Form: December 8, 1999

The ionization bands and electron affinities of medium-size B_nN_n clusters ($n = 3, 4, 5$) have been investigated by means of one-particle Green's function calculations using the outer-valence Green's function (OVGF) approximation or the third-order algebraic diagrammatic construction [ADC(3)] scheme. Despite their structural similarity with isoelectronic cumulenic carbon chains and rings, these clusters do not exhibit a significant breakdown of the orbital picture of ionization, with the exception of the N_{2s} bands ($\epsilon_b > 25$ eV), which relate exclusively to complex sets of shake-up lines. The main (one-hole) ionization bands provide specific signatures for ring topologies based on ***n*** equivalent vertices, whereas a reduction of the curvature of N−B−N bridges with increasing system size can be followed from the N_{2s} bands. The $B_3N_3^-$ anion is slightly stable against electron loss, whereas negative vertical electron affinities are obtained for B_4N_4 and B_5N_5.

1. Introduction

Mixed boron−nitrogen clusters are nowadays arousing considerable interest as precursors in the growth of β-BN thin films using chemical vapor deposition or plasma techniques.[1] Intensive research is conducted in order to synthesize the sphalerite-type (or β-crystalline phase) of boron nitride, which is isostructural and isoelectronic to cubic diamond and displays[1−3] exceptional physicochemical properties (e.g., mechanical hardness, thermal stability and conductivity, chemical stability with respect to ferrous alloys, the possibility of n or p doping, and the emission of blue light at the p−n junction). Many experimental studies point out a tricky dependence[4] of the phase distribution and chemical composition of the deposited material on the composition of the plasma, the components of which are thermally excited B_n, N_m, B_nN_m neutral species, as well as their positive and negative ions. A sound characterization of the ionization and electron attachment properties of such clusters is thus essential to carry out a reliable plasma diagnostics in BN coating. In addition, investigations on boron−nitrogen clusters are topical in regard to the existence of fullerene analogues involving B and N atoms.[5−7]

Small boron−nitrogen species such as BN, B_2N, BN_2, B_2N_2, B_3N, BN_3, B_3N_2, and B_2N_3 have been the subject of a number of high-level theoretical investigations[8−14] of their structural, vibrational (BN_4), thermochemical, dissociation or spectroscopic properties. Theoretical predictions[8] of the structure and reactivity of B_2N and BN_2 have been furthermore confirmed in pulsed laser evaporation experiments combined with matrix infrared spectroscopy.[11,15] Of relevance also is an experimental characterization of B_2N and BN_2 by electron spin resonance.[16]

Data on larger boron−nitrogen clusters are particularly limited both in abundance and accuracy. Theoretical studies[17] of B_nN_n clusters ($n = 3−10$) using density functional theory (DFT) with the hybrid B3LYP functional unequivocally indicate monocyclic rings of D_{nh} symmetry and with sharp BNB and dull NBN bond angles to be by far the most stable structures. These calculations are consistently supported by investigations of the molecular structures of B_3N_3 and B_4N_4 at the UMP2[18] and CCSD(T)[19] levels (i.e., unrestricted second-order Møller−Plesset perturbation theory and coupled cluster Ansatz with all single and double excitations and a quasiperturbative treatment of connected triple excitations, respectively). The lowest electronic state of B_nN_n clusters ($n = 3−10$) is invariably found[17−19] to be a singlet closed shell. On the contrary, for B_2N_2, UMP2 theory gives[18] as most stable and nearly isoenergetic forms rhombus (D_{2h}) and linear ($D_{\infty h}$) structures, both with a triplet state as lowest electronic state.

Except for rather questionable UMP2 estimates[18] of the vertical ionization threshold of BN (12.5 eV), B_2N_2 (9.9 eV), B_3N_3 (11.7 eV), and B_4N_4 (9.8 eV), nothing is known about the ionization and electron-attachment properties of mixed boron−nitrogen clusters. The present investigation aims first at providing a complete survey of the primary one-hole (1h) and excited two-hole-one-particle (2h-1p) shake-up configurations associated to the vertical ionization spectra of closed-shell B_nN_n species. This study is carried out by means of accurate and efficient schemes derived within the framework of the one-particle Greens's function (1p-GF) theory,[20,21] coping with electronic correlation *through* third-order in many-body perturbation theory. As a byproduct, the same schemes are also used to evaluate vertical electron affinities. The present article deals with the B_nN_n ($n = 3, 4, 5$) clusters, which are isoelectronic with the cyclic C_{2n} ($n = 3, 4, 5$) clusters,[22] and are also characterized by the conjugation of n out-of-plane π-electrons and n in-plane pseudo-π electrons. Since the main characteristic of B_nN_n rings is a fully regular (i.e., nonalternating) pattern of

10.1021/jp993232x CCC: $19.00
Published on Web 02/01/2000

B−N bonds, it will be interesting to compare the results presented here with recent 1p-GF investigations of the ionization spectra of closed-shell and cumulenic linear C_{2n-1} ($n = 2-5$)[23,24] or cyclic C_{2n} ($n = 3, 5$)[25] clusters.

2. Computational Methods

One-particle Green's function (1p-GF) calculations have been performed using the so-called third-order algebraic diagrammatic construction [ADC(3)] scheme[26,27] and the simpler outer-valence Green's function (OVGF) approximations,[20,28,29] using Dunning's cc-pVDZ (correlation consistent polarized valence double-ζ) basis set,[30] which is a [3s2p1d] contraction of a (9s4p1d) primitive set. The selected structures were optimized[17] at the B3LYP/cc-pVDZ level, an approach which is known[31] to provide geometries (and vibrational frequencies) of quality comparable to that of a CCSD(T) treatment[32] (coupled cluster Ansatz, including single, double excitations, and a perturbative estimate of triple excitations − a benchmark for most quantum-chemical studies). By extrapolation of 1p-GF results based on larger basis sets and obtained for the closely related cumulenic carbon clusters,[23−25] these levels of theory should be more than sufficient for evaluating quantitatively one-electron binding energies and the extent of the shake-up contamination in the spectra of B_nN_n ($n = 3-5$) species.

More specifically, the OVGF approach employs[20,28] diagonal second- and third-order self-energy diagrams in a geometric approximation to the poles of the Green's function. It thus enables a consistent treatment of the primary 1h ionization and 1p electron attachment energies *through* third-order in electron correlation, but fails in providing accurate ionization energies and intensities when close-by excited (shake-*up* or shake-*on*) states appear. It is completely inapplicable when one-hole cation states can no longer be distinguished from their shake-up satellites, a situation which is most commonly referred to as a "*complete breakdown of the orbital picture of ionization*".[21] For a consistent and quantitative treatment of 1h and 2h-1p ionized states throughout the valence region, one must at least consider calculations at the 1p-GF/ADC(3)[21,24,26] or comparable[23,33] levels.

The latter approaches can be summarized as an advantageous compromise between the construction principles of the configuration interaction (CI) and many-body perturbation theories (MBPT). They retain in particular the property of *size-consistency*[33] associated with linked-cluster diagrammatic expansions of self-energies, but at the same time incorporate a multistate (CI-like) treatment of excited configurations. Specifically, besides a description of one-electron ionization or attachment processes being exact *through* third-order in correlation, 1p-GF/ADC(3) enables a *through* first-order multistate treatment of the shake-*up* (2h-1p) cation states and of the shake-*on* (2p-1h) anion states. The latter is equivalent to the so-called two-particle-hole Tamm−Dankoff renormalization[34] of an infinite series of self-energy diagrams of mixed RPA-ladder character.[20] At the 1p-GF/ADC(3) level, the couplings of the 2h-1p (2p-1h) states with the 1h (1p) states are of second order.[26] The interested reader is referred further to refs 25 and 33−41, and references therein, for the practical aspects and other essential features (systematic compactness, size intensivity, charge consistency, etc.) of these Green's function methods when applied on large molecular chains or clusters.

In the present work, attention has also been focused on the first vertical electron affinity, in order to evaluate the stability of $B_nN_n^-$ anions against electron loss. Although these can also be, in principle, obtained directly using the 1p-GF/ADC(3) scheme, we did not seek in this work both the computationally very demanding computation of electron affinities associated with 2p-1h shake-*on* processes, and an exhaustive investigation of the energies of unoccupied one-electron bound states.

The Hartree−Fock (HF) entries required for the 1p-GF/ADC-(3) package have been obtained from SCF calculations carried out by means of the GAMESS-US series of programs.[42] The requested convergences on each of the elements of the HF density matrix and the integral cutoff were fixed to 10^{-5} and 10^{-9} hartree, respectively. In the present work, only ionization lines with a pole strength larger than 0.005 have been extracted in the final (block-Davidson) diagonalization step of the 1p-GF/ADC(3) computations. OVGF calculations, on the other hand, have been performed using the *Gaussian 98* package.[43] The basis set contention of the results obtained for the vertical ionization potentials and electron affinities has been assessed by comparison with OVGF calculations using the augmented cc-pVDZ basis set,[44] which is a [4s3p2d] contraction of a (10s5p2d) primitive set, comprising one set of diffuse (spd) functions.

The simulated spectra presented in the sequel are constructed from a convolution of the 1p-GF/ADC(3) ionization lines, using as spread function a linear combination of one Lorentzian and one Gaussian curve of equal weight and width (fwhm = 1.1 eV). The intensities are scaled according to the spectroscopic pole strengths, i.e., without any consideration of photoionization cross sections.

3. Results and Discussion

3.1. Structural and Topological Considerations. Results obtained at the HF/cc-pVDZ and 1p-GF/ADC(3)/cc-pVDZ levels for the ionization energies of B_3N_3, B_4N_4, and B_5N_5 and the related spectroscopic strengths are presented in Tables 1−3 and displayed as spike spectra and in convoluted forms in Figures 1a−c and 2a−c, successively. The HF (Figure 1) and the 1p-GF/ADC(3) (Figure 2) spectra reflect a clear partition of the 4*n* valence electron orbitals of a B_nN_n ($n = 3, 4, 5$) ring into *n* well-defined "inner valence" orbitals (of which Int[$(n-1)/2$][45] doubly degenerate sets) of leading N_{2s} character at high binding energies (i.e., above 25 eV), and 3*n* orbitals of mixed B_{2s}, B_{2p}, and N_{2p} character at lower ("outer-valence") binding energies (i.e., below 20 eV). This very peculiar partition can be directly related to the very low binding energy of 2s electrons in a boron atom (14.77 eV, from HF/cc-pVDZ data), which is practically identical to that of 2p electrons in a nitrogen atom (14.99 eV, at the same level).

The lowest "outer-valence" HF levels of the B_nN_n clusters correspond (Tables 4−6) to orbitals (of which Int[$(n-1)/2$] doubly degenerate sets) of leading $B_{2s} + N_{2p}$ or mixed $B_{2s} + B_{2p} + N_{2p}$ character (which for simplicity will be referred to as $B_{2s} + N_{2p}$ levels), whereas the outermost 2*n* orbitals are clearly dominated by B_{2p} and N_{2p} contributions. The latter can be further divided into two overlapping sets of *n* orbitals, one of Σ symmetry, and the other one of Π symmetry, with for each set Int[$(n-1)/2$] pairs of degenerate levels. This is consistent with the cumulenic-like depiction of 2*n* double bonds, i.e., the conjugation of *n* out-of-plane π-electrons and *n* in-plane pseudo-π electrons, in cyclic structures exhibiting ***n*** topologically equivalent sharp B−N−B vertices and quasilinear N−B−N bridges.[17−19]

Rather unsurprisingly, therefore, the 1:2, 1:2:1, and 1:2:2 multiplicity distributions invariably observed among the N_{2s}, Σ-B_{2p}−N_{2p}, and Π-B_{2p}−N_{2p} HF energy levels of, successively, B_3N_3 (Table 1), B_4N_4 (Table 2), and B_5N_5 (Table 3) can be easily recovered from a tight-binding (or extended Hückel)

TABLE 1: Vertical Electron Affinity and Ionization Potentials (in eV) Obtained for B_3N_3 (D_{3h} Symmetry Group) together with the Corresponding Pole Strength (in parentheses)[a]

level	HF/ cc-pVDZ	ADC(3)/ cc-pVDZ	OVGF/ cc-pVDZ	OVGF/ aug-cc-pVDZ
$5a_1'$	−0.660		+0.464 (0.936)	+0.807 (0.948)
$1e''$	11.582	11.038 (0.895)	10.924 (0.904)	11.170 (0.898)
$5e'$	13.143	11.890 (0.889)	11.805 (0.897)	12.007 (0.892)
$1a_2''$	15.734	14.673 (0.843)	14.618 (0.885)	14.839 (0.880)
		18.915 (0.025)		
$1a_2'$	16.600	15.345 (0.797)	15.170 (0.904)	15.385 (0.899)
		15.647 (0.098)		
$4a_1'$	17.401	15.826 (0.845)	15.552 (0.873)	15.710 (0.868)
$4e'$	17.949	16.186 (0.053)	16.550 (0.901)	16.733 (0.897)
		16.845 (0.832)		
$3e'$	31.632	26.553 (0.047)		
		26.885 (0.021)		
		26.997 (0.021)		
		27.294 (0.043)		
		27.313 (0.101)		
		27.511 (0.109)		
		28.822 (0.045)		
		28.900 (0.065)		
		28.954 (0.020)		
		28.998 (0.066)		
$3a_1'$	33.973	27.448 (0.025)		
		28.294 (0.020)		
		28.453 (0.026)		
		28.902 (0.095)		
		29.713 (0.024)		
		29.809 (0.024)		
		29.935 (0.054)		
		30.324 (0.061)		
		30.542 (0.135)		
		30.582 (0.047)		
		30.930 (0.024)		
		30.436 (0.100)		
		33.668 (0.030)		

[a] Only the lines with $\Gamma > 0.02$ are listed.

TABLE 2: Vertical Electron Affinity and Ionization Potentials (in eV) Obtained for B_4N_4 (D_{4h} Symmetry Group) together with the Corresponding Pole Strength (in parentheses)[a]

level	HF/ cc-pVDZ	ADC(3)/ cc-pVDZ	OVGF/ cc-pVDZ	OVGF/ aug-cc-pVDZ
$5a_{1g}$	−2.446		−1.148 (0.929)	−0.348 (0.979)
$1b_{1u}$	10.426	9.629 (0.892)	9.564 (0.899)	9.860 (0.894)
$3b_{2g}$	12.252	11.073 (0.888)	10.984 (0.894)	11.224 (0.889)
$1e_g$	13.267	12.345 (0.881)	12.232 (0.893)	12.471 (0.888)
$5e_u$	14.092	12.852 (0.883)	12.687 (0.888)	12.901 (0.883)
$1a_{2u}$	15.562	14.349 (0.841)	14.315 (0.883)	14.545 (0.878)
		19.509 (0.025)		
$4a_{1g}$	17.037	15.497 (0.692)	15.322 (0.874)	15.497 (0.869)
		15.867 (0.148)		
$1a_{2g}$	17.439	16.166 (0.898)	15.705 (0.897)	15.946 (0.892)
$4e_u$	18.538	17.294 (0.832)	16.829 (0.895)	17.038 (0.890)
		17.598 (0.064)		
$2b_{1g}$	19.468	18.164 (0.760)	17.776 (0.893)	17.958 (0.889)
		18.223 (0.073)		
		18.879 (0.042)		
$2b_{2g}$	31.545	26.758 (0.044)		
		27.246 (0.031)		
		27.385 (0.120)		
		27.496 (0.111)		
		27.586 (0.097)		
		27.834 (0.022)		
		28.778 (0.034)		
		29.003 (0.088)		
		29.065 (0.024)		
		29.272 (0.040)		
		29.702 (0.034)		
$3e_u$	32.191	28.015 (0.119)		
		28.233 (0.028)		
		28.692 (0.020)		
		28.935 (0.076)		
		29.390 (0.037)		
		29.483 (0.028)		
		29.559 (0.025)		
		30.316 (0.030)		
		30.804 (0.028)		
$3a_{1g}$	33.184	26.921 (0.028)		
		27.806 (0.032)		
		28.263 (0.027)		
		28.564 (0.035)		
		28.630 (0.029)		
		28.770 (0.067)		
		29.875 (0.106)		
		29.920 (0.028)		
		30.259 (0.035)		
		30.416 (0.097)		
		30.607 (0.021)		
		32.813 (0.023)		

[a] Only the lines with $\Gamma > 0.02$ are listed.

picture and applications of elementary graph theory[46] on cyclic topologies based on 3, 4, and 5 vertices, as suggested in Figure 3. However, inversion of the 1:2 and 1:2:2 multiplicity patterns inferred from connectivity only can be noticed (Tables 1 and 3) for the $B_{2s}-N_{2p}$ sets of B_3N_3 and B_5N_5. Furthermore, the calculated HF spectra (Figure 1) clearly reflect a very unusual reduction of the energy spreading of the inner-valence N_{2s} levels with increasing system size. At last, relaxation effects appear to affect nonuniformly the shape and width of bands in the 1p-GF/ADC(3) spectra (see section 3.2). These observations indicate strong inhomogenities within the electronic structure of B_nN_n compounds, and call for further analysis at the HF level.

Contour plots of the 12 valence orbitals of B_3N_3 are displayed in Figure 4. Clearly, some of these orbitals ($3a_1'$, $4e'$, $5e'$, $1e''$) present features typical of 3-center N−B−N chemical bonds. In addition, and as clearly shown with orbitals $4a_1'$ and $5e'$, the B_3N_3 ring also affords internal and delocalized chemical bondings over its equilateral triangle of boron atoms, the dimensions of which approach that of the B_3 molecule.[8] A detailed analysis (Tables 4−6) of the atomic composition of the N_{2s} levels of B_nN_n rings reveals a substantial proportion of B_{2s} contributions, up to 36% for the $3a_1'$ orbital of B_3N_3. For this molecule, the bending of the N−B−N bridges (θ_{NBN} = 152.1°[17]) clearly enhances the effect of through-bond interactions between the N_{2s} atomic functions, and ultimately results in an energy splitting of the N_{2s} levels by ΔE = 2.34 eV. Interestingly, the importance of the B_{2s} contamination of the inner-valence N_{2s} bands tends to slightly but significantly reduce with increasing system size (Tables 4−6), whereas the N−B−N bridges approach linearity (θ_{NBN} = 169.2° in B_4N_4, 173.0° in B_5N_5, up to 179.4° in B_9N_9[17]). Conversely, an increase in the B_{2s} content of the innermost $B_{2s} + N_{2p}$ lines is globally observed, which is consistent with the idea of an $sp^2 \rightarrow sp$ rehybridation of boron atoms in the largest B_nN_n rings. For these rings, the final outcome of the orbital content and of the enhanced separation of N atoms is thus a substantial release of through-bond $N_{2s}-N_{2s}$ overlaps. This corroborates the reduction of the energy spreading of the n innermost levels of B_nN_n compounds, from ΔE = 1.64 eV with B_4N_4, ΔE = 1.12 eV for B_5N_5, up to ΔE = 0.91 eV when considering B_9N_9.

The reversal of the multiplicity pattern of the $B_{2s} + N_{2p}$ levels can be rather easily explained through orbital topologies. A fully symmetric combination of B_{2s}, B_{2p}, and N_{2p} atomic functions such as the $4a_1'$ orbital of B_3N_3 (Figure 4f) is rather unfavorable, since with its circular nodal plane following closely the B−N backbone it tends very generally to deprive the regions

TABLE 3: Vertical Electron Affinity and Ionization Potentials (in eV) Obtained for B_5N_5 (D_{5h} Symmetry Group) together with the Corresponding Pole Strength (in parentheses)[a]

level	HF/ cc-pVDZ	ADC(3)/ cc-pVDZ	OVGF/ cc-pVDZ	OVGF/ aug-cc-pVDZ
$5a_1'$	−3.223		−2.076 (0.945)	−0.306 (0.978)
$1e_2''$	11.127	10.232 (0.885)	10.175 (0.894)	10.447 (0.889)
$5e_2'$	12.356	11.096 (0.880)	11.085 (0.889)	11.306 (0.884)
$1e_1''$	14.016	12.923 (0.862)	12.881 (0.887)	13.105 (0.882)
$5e_1'$	14.654	13.291 (0.861)	13.257 (0.882)	13.452 (0.877)
$1a_2''$	15.363	14.089 (0.841)	14.088 (0.880)	14.308 (0.876)
$4a_1'$	16.368	14.902 (0.840)	14.883 (0.875)	15.080 (0.870)
$1a_2'$	18.094	16.310 (0.878)	16.187 (0.891)	16.415 (0.886)
$4e_1'$	18.879	17.134 (0.865)	16.996 (0.889)	17.205 (0.885)
$4e_2'$	20.007	18.184 (0.397)	18.146 (0.887)	18.323 (0.883)
		18.355 (0.427)		
$3e_2'$	31.609	27.141 (0.022)		
		27.193 (0.135)		
		27.252 (0.158)		
		27.417 (0.028)		
		27.790 (0.026)		
		28.748 (0.051)		
		28.855 (0.022)		
		29.039 (0.042)		
$3e_1'$	32.260	27.596 (0.050)		
		27.682 (0.030)		
		27.776 (0.098)		
		27.864 (0.021)		
		29.057 (0.024)		
		29.181 (0.022)		
		29.218 (0.028)		
		29.319 (0.068)		
		29.575 (0.026)		
$3a_1'$	32.728	27.922 (0.027)		
		28.135 (0.047)		
		28.214 (0.110)		
		28.709 (0.020)		
		29.347 (0.044)		
		29.557 (0.106)		
		29.679 (0.039)		
		29.803 (0.033)		

[a] Only the lines with $\Gamma > 0.02$ are listed.

associated with the chemical bonds of electrons, pushing these outside the B_nN_n ring. On the other hand, less symmetric orbitals such as the 4e′ orbitals of B_3N_3 (Figures 4d,e) enable a more energetically favorable LCAO combination of B_{2s} and N_{2p} functions which maximizes and delocalizes electron densities between the B and N atoms. These observations on the $B_{2s} + N_{2p}$ orbitals can be extended to larger B_nN_n rings, since their stability appears to conversely follow the number of nodal planes, as can be inferred from the symmetry labels (see, e.g., Table 3). Very generally, from their topology and in view of their atomic N_{2s} and N_{2p} content (Tables 4−6), the outermost fully symmetric orbitals ($4a_1'$ in B_3N_3, $4a_{1g}$ in B_4N_4, $4a_1'$ in B_5N_5) can be regarded as the lowest in plane lone-pair nitrogen orbital. Other levels that relate to the remaining $n - 1$ nitrogen lone-pairs and participate to the in-plane (or pseudo-Π) conjugation are the outermost sets of Σ-symmetry (5e′ in B_3N_3, $3b_{2g}$ and $1e_g$ in B_4N_4, $5e_1'$ and $5e_2'$ in B_5N_5).

3.2. One-Hole Ionization Lines and Bands. Inclusion of many-body effects via the 1p-GF/ADC(3) or OVGF approaches does not yield a reordering of the binding energies pertaining to the one-hole or one-particle $B_{2s}-B_{2p}-N_{2p}$ levels, compared with the HF/Koopmans' results (Tables 1−3). These approaches invariably indicate, as first cation state, a doubly degenerate set of one-hole levels of "Π" symmetry.

As could be expected, electron relaxation and correlation do not affect in a strikingly different way the ionization energies

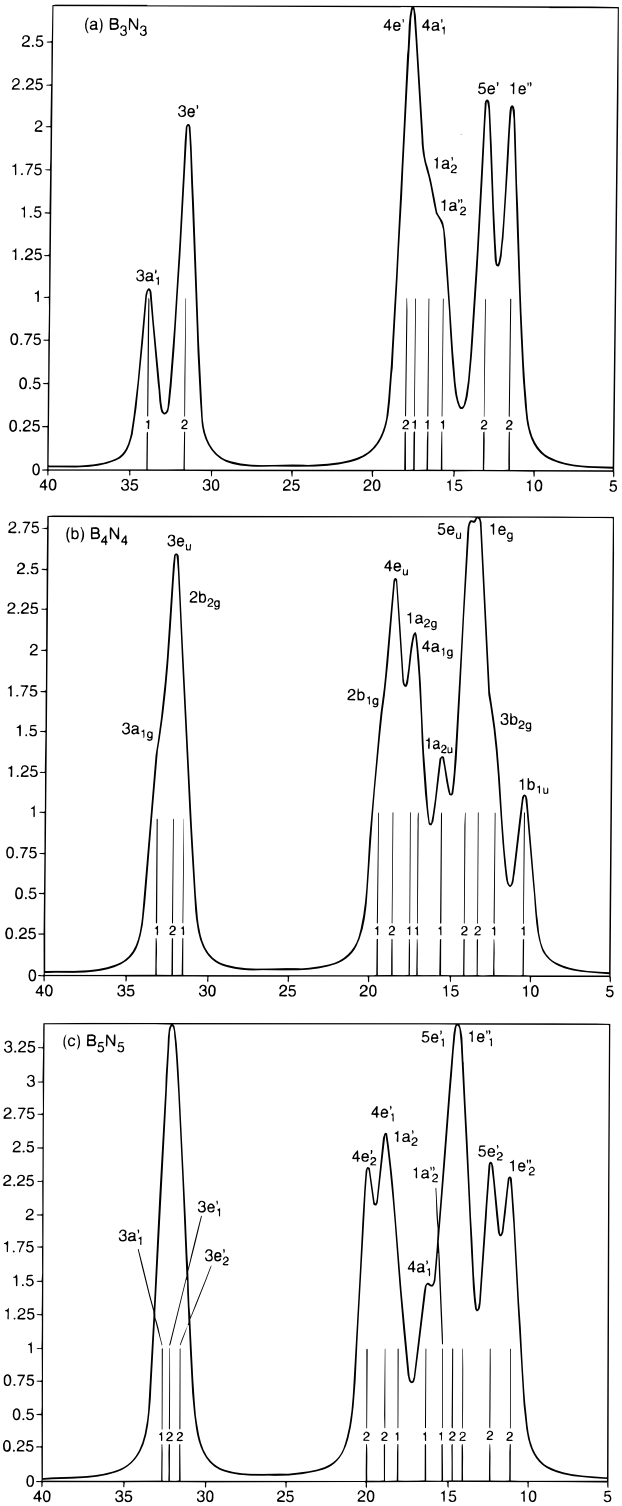

Figure 1. HF ionization spectra (pole strengths or convoluted spectral intensities versus binding energies, in eV) of (a) B_3N_3, (b) B_4N_4, and (c) B_5N_5 (results obtained using a cc-pVDZ basis set). Line multiplicities are superposed onto the spike spectrum.

associated with the $B_{2p}-N_{2p}$ π out-of-plane and pseudo-π in-plane conjugation systems, especially when considering the largest B_nN_n rings. More specifically, the magnitude of these effects on the highest occupied $B_{2p}-N_{2p}$ π out-of-plane molecular orbital is found to gently increase with the size of the B_nN_n rings [$\Delta IP(1e''/B_3N_3) = -0.54$ eV; $\Delta IP(1b_{1u}/B_4N_4) = -0.80$ eV, $\Delta IP(1e_2''/B_5N_5) = -0.90$ eV, see the HF and

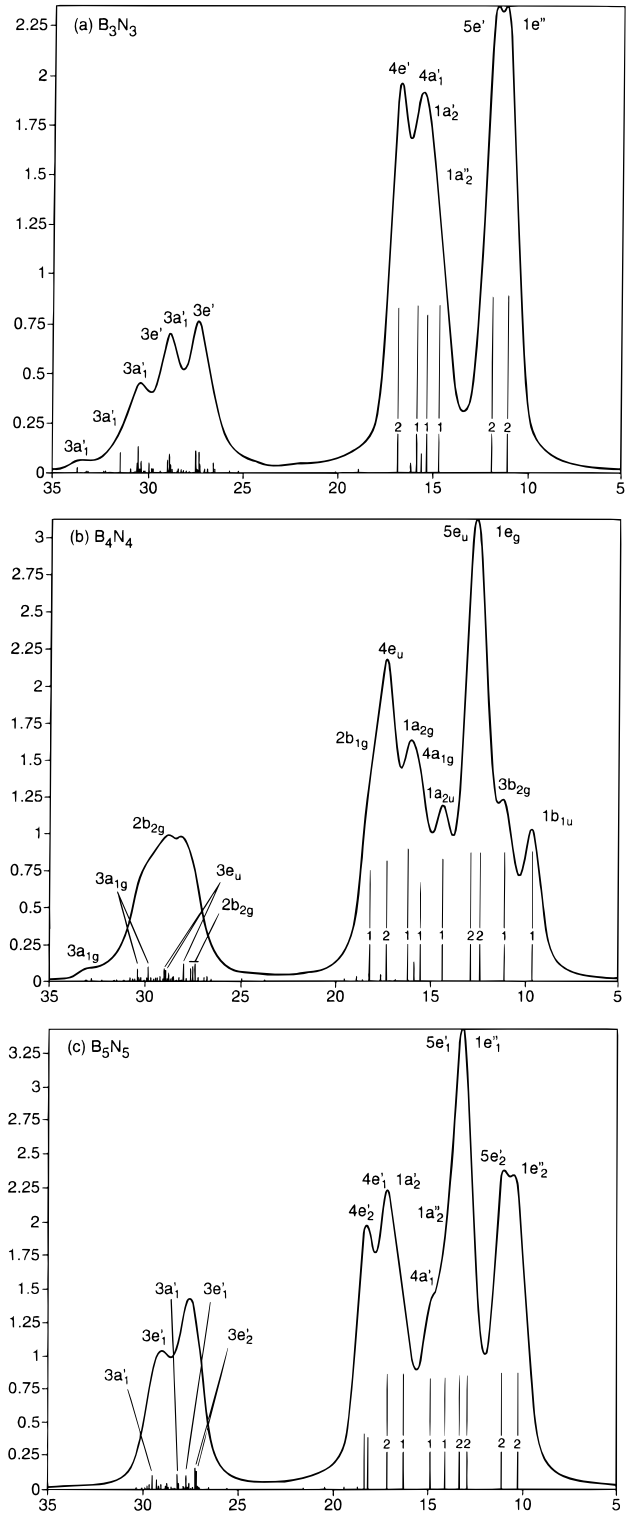

Figure 2. 1p-GF/ADC(3) ionization spectra (pole strengths or convoluted spectral intensities versus binding energies, in eV) of (a) B_3N_3, (b) B_4N_4, and (c) B_5N_5 (results obtained using a cc-pVDZ basis set). Line multiplicities for the primary 1h ionization states are superposed onto the spike spectrum.

ADC(3) data in Tables 1−3], whereas they remain practically constant for the highest occupied $B_{2p}-N_{2p}$ pseudo-π in-plane orbital [$\Delta IP(5e'/B_3N_3) = -1.25$ eV; $\Delta IP(3b_{2g}/B_4N_4) = -1.18$ eV, $\Delta IP(5e_2'/B_5N_5) = -1.26$ eV]. Overall, electron correlation and relaxation effects on one-hole ionization lines result in shifts toward lower binding energies and comprised between 0.8 and 1.5 eV. A comparison of the spectra displayed in Figures 1 and 2 shows very generally a broadening of the innermost B_{2s}-(+B_{2p})+N_{2p} bands, and on the contrary a sharpening of the outermost $B_{2p}-N_{2p}$ bands upon inclusion of electron correlation and relaxation. The effect of electron relaxation on the energy interval between the 4e′ [$\Delta IP = -1.1$ eV] and $4a_1'$ [$\Delta IP = -1.56$ eV] levels of B_3N_3 is particularly noteworthy [$\Delta E = 0.55$ eV at the HF level; $\Delta E = 1.02$ eV at the ADC(3) level], and obviously relates to the lone-pair, and therefore more strongly localized character of the latter level. Similarly, and for the same reasons, the $4a_{1g}$ and $4a_1'$ lines of B_4N_4 and B_5N_5 distinguish themselves by significant shifts from the HF to the ADC(3) spectra [$\Delta IP = -1.54$ and -1.46 eV, respectively].

Despite the non uniformity of relaxation effects, the $B_{2s}-B_{2p}-N_{2p}$ ionization bands displayed in the ADC(3) spectra of Figure 2 are rather similar, in shape and intensity, to those obtained at the HF level (Figure 1). Although the ADC(3) ionization spectra obtained up to B_5N_5 (Figure 2) are still quite far from fully converging to a limiting profile, extrapolation of 1p-GF/ADC(3) and OVGF results to larger B_nN_n rings indicates that their convoluted $B_{2s}-B_{2p}-N_{2p}$ bands will display three peaks at about 17, 14, and 10 eV. In view of the multiplicity

TABLE 4: Detailed Analysis of the Valence Orbital Structure of B_3N_3[a]

orbitals	% B_{2s}	% N_{2s}	% B_{2p}	% N_{2p}
$1e''$ (Π)	0	0	**21**	**77**
$5e'$ (Σ)	6	10	**16**	**55**
$1a_2''$ (Π)	0	0	**44**	**52**
$1a_2'$ (Σ)	0	0	**49**	**45**
$4a_1'$ (Σ)	9	25	22	**34**
$4e'$ (Σ)	**43**	1	10	**38**
$3e'$ (Σ)	9	**58**	20	3
$3a_{1'}$ (Σ)	36	**45**	4	4

[a] Percentages of N_{2s}, N_{2p}, B_{2s}, or B_{2p} atomic contribution. Character of orbitals are evaluated from their LCAO coefficients.

TABLE 5: Detailed Analysis of the Valence Orbital Structure of B_4N_4

orbitals	% B_{2s}	% N_{2s}	% B_{2p}	% N_{2p}
$1b_{1u}$ (Π)	0	0	0	**97**
$3b_{2g}$ (Σ)	0	8	**17**	**63**
$1e_g$ (Π)	0	0	**29**	**69**
$5e_u$ (Σ)	11	11	**18**	**52**
$1a_{2u}$ (Π)	0	0	**40**	**57**
$4a_{1g}$ (Σ)	8	19	**27**	**39**
$1a_{2g}$ (Σ)	0	0	**49**	**44**
$4e_u$ (Σ)	25	1	**27**	**39**
$2b_{1g}$ (Σ)	57	0	2	**36**
$2b_{2g}$ (Σ)	0	**61**	27	2
$3e_u$ (Σ)	19	**55**	15	3
$3a_{1g}$ (Σ)	34	**52**	1	3

TABLE 6: Detailed Analysis of the Valence Orbital Structure of B_5N_5

orbitals	% B_{2s}	% N_{2s}	% B_{2p}	% N_{2p}
$1e_2''$ (Π)	0	0	**10**	**88**
$5e_2'$ (Σ)	2	7	**15**	**64**
$1e_1''$ (Π)	0	0	**32**	**66**
$5e_1'$ (Σ)	10	10	**21**	**53**
$1a_2''$ (Π)	0	0	**38**	**59**
$4a_1'$ (Σ)	7	14	**27**	**47**
$1a_2'$ (Σ)	0	0	**50**	**42**
$4e_1'$ (Σ)	**17**	1	**34**	**39**
$4e_2'$ (Σ)	**50**	0.4	7	**37**
$3e_2'$ (Σ)	4	**61**	24	2
$3e_1'$ (Σ)	23	**57**	9	2
$3a_1'$ (Σ)	33	**55**	0.5	2

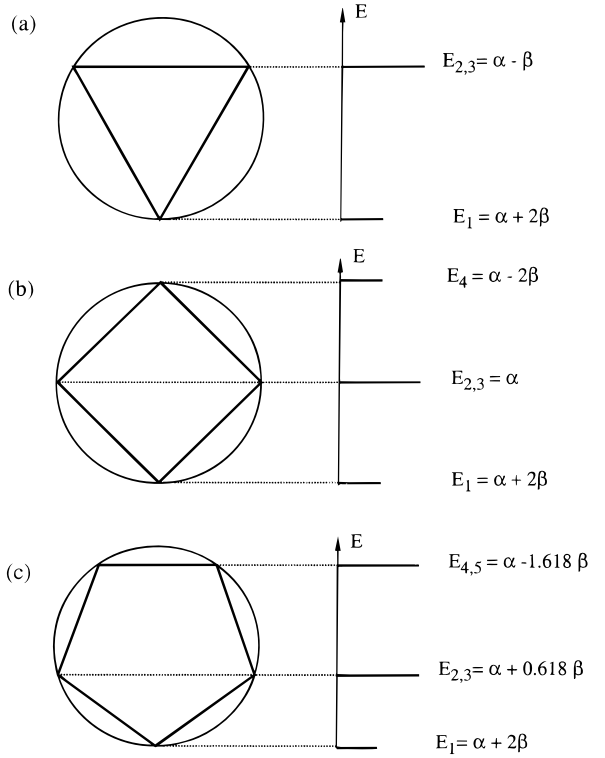

Figure 3. Hückel energy diagrams corresponding to rings of (a) 3, (b) 4, and (c) 5 equivalent vertices.

and energy distribution of the Σ and Π $N_{2p} + B_{2p}$ lines, the central peak at 14 eV should distinguish itself both by its sharpness and intensity.

3.3. Shake-Up Ionization Lines and Bands. The most striking feature of the 1p-GF/ADC(3) ionization spectra (Figure 2) is the strong fragmentation of the N_{2s} ionization lines into complex sets of 2h-1p shake-up states. Since no clearly dominant one-hole cation state can be distinguished within these sets, the orbital picture of ionization within the N_{2s} bands can be regarded as fully breaking down. Extrapolation of trends to larger clusters shows that shake-up lines in the N_{2s} bands should dilute into a continuum of lines with vanishingly small intensity in the limit of an infinitely large ring. From straightforward implications[40] of translational symmetry in periodic systems with cyclic boundary conditions, the number of 2h-1p shake-up satellites to identify per orbital in the inner valence region has to increase as n^2, whereas their individual averaged intensity must scale like n^{-2}.[41] Very obviously, the breakdown of the orbital picture of ionization leads to a considerable broadening of the N_{2s} bands.

Despite this, and despite the multiplication of shake-up lines or peaks, the 1:2 multiplicity ratio between the $3a_1'$ and $3e'$ levels of B_3N_3 and the 1:2:2 multiplicity ratios of the $3a'_1$, $3e'_1$, and $3e'_2$ orbitals of B_5N_5 are still recognizable (Figures 2a and 2c) from a global asymmetry of the N_{2s} band. Conversely, the 1:2:1 multiplicity ratios of the $2b_{2g}$, $3e_u$, and $3a_{1g}$ levels of B_4N_4 are clearly marked by a more symmetric profile for the N_{2s} band. Furthermore, like the HF energy distributions from which they derive, the 1p-GF/ADC(3) spectra still portend the effect of through-bond $N_{2s}-(B_{2s})-N_{2s}$ interactions in the form of a striking reduction of the energy spreading of N_{2s} lines (Figures 2, Tables 1−3) with increasing system size.

Unlike pure carbon chains[24] or rings,[25] shake-up lines play a very limited role within the "outer valence" bands of B_nN_n compounds. Comparison of the ADC(3) spectrum of the B_5N_5 species (Figure 2c) with those obtained (Figures 2a and 2b) for smaller rings (B_3N_3, B_4N_4) indicates that the onset of shake-up contamination is confined to the bottom of the outer-valence band (i.e., at 15.6 eV for B_3N_3, 15.9 eV for B_4N_4, and 18.2 eV for B_5N_5). One can notice however a splitting of the first ($4e_2'$) one-hole $B_{2s} + N_{2p}$ line of B_5N_5 (Table 3) into two shake-up lines with comparable strength, at 18.18 eV ($\Gamma = 0.397$) and 18.36 eV ($\Gamma = 0.427$).

Quite importantly, it must be reminded that carbon chains or rings represent the only case reported so far[24,25] where outer-valence ionization lines of Π character are found to be affected by a severe breakdown of the orbital picture of ionization. This can be related to the strongly correlated nature of clusters with low-lying orbitals of Π symmetry. In view of their cumulenic character, carbon chains or rings should display a vanishingly small band gap and thus metallic properties in the limit of an infinitely large structure. On the other hand, the strong polarity of B−N chemical bonds results very naturally in an intrinsic alternation of the electron density (see e.g., the charge density plots in ref 18), and a substantial opening of the HOMO−LUMO HF band gap (from 12.24 eV in B_3N_3, to 14.35 eV in B_5N_5). Furthermore, unlike carbon clusters, the lowest virtual orbital of B_3N_3, B_4N_4, and B_5N_5 belongs to the fully symmetic irreducible representation of the D_{3h}, D_{4h} and D_{5h} symmetry point groups, successively (Tables 1−3). Since the HOMO is of Π-type, this strongly impedes (and in practice strictly forbids) couplings of 1h lines to shake-up transition of the $HOMO^{-2}$ $LUMO^{+1}$ type.[38,40] For these species, the lowest unoccupied levels of Π symmetry ($2e''$, $1b_{2u}$, $2e_2''$) appear furthermore to be rather high lying in energy (from the HF/cc-pVDZ results, at 4.67, 2.93, and 3.56 eV above the vacuum level, successively). Despite their structural similarity with isolectronic cumulenic carbon chains and rings, medium-size and large B_nN_n species are thus characterized by a clear limitation of their propensity for electronic excitations in general.

3.4. Basis Set Contention. The OVGF/cc-pVDZ results closely follow the values obtained for 1h ionization energies and their associated pole strength at the 1p-GF/ADC(3)/cc-pVDZ level (Tables 1−3). Discrepancies between the two approaches appear overall to increase from ∼0.1 up to ∼0.4 eV from the top to the bottom of the $B_{2s}-B_{2p}-N_{2p}$ valence bands, in relationship with the appearance of a few shake-up lines in this energy region. With a systematic but very weak underestimation, by ∼0.18 to ∼0.30 eV only, of the values obtained for 1h ionization energies at the OVGF/aug-cc-pVDZ level, the OVGF/cc-pVDZ results conclusively show that inclusion of diffuse functions is relatively unimportant for the description of ionization spectra. On the other hand, a comparison of the OVGF/cc-pVDZ and OVGF/aug-cc-pVDZ results (Tables 1−3) reveals an extremely strong basis set dependence (up to 1.74 eV) of electron affinities. Although it is well-known that inclusion of polarization and diffuse functions is very necessary to describe anion bound states close to or embedded within the continuum, the importance of the basis set dependence of the electron affinities of B_nN_n clusters compared to that of C_n species[23,25] is at first glance very surprising. In this case, the problem is complicated by the strong polarity of the investigated species.

3.5. First Anion States and Electron Affinities. All possible combinations of the methods (HF, OVGF) and basis sets in use in the present work invariably indicate as lowest anion state a nondegenerate and fully symmetric one-particle state. Further topological analysis of the lowest unoccupied molecular orbital (LUMO) obtained for B_3N_3 and B_4N_4 (Figures 5a and b) at the HF/cc-pVDZ level and decomposition in terms of its LCAO coefficients (Table 7) point out a dominant in-plane, outward

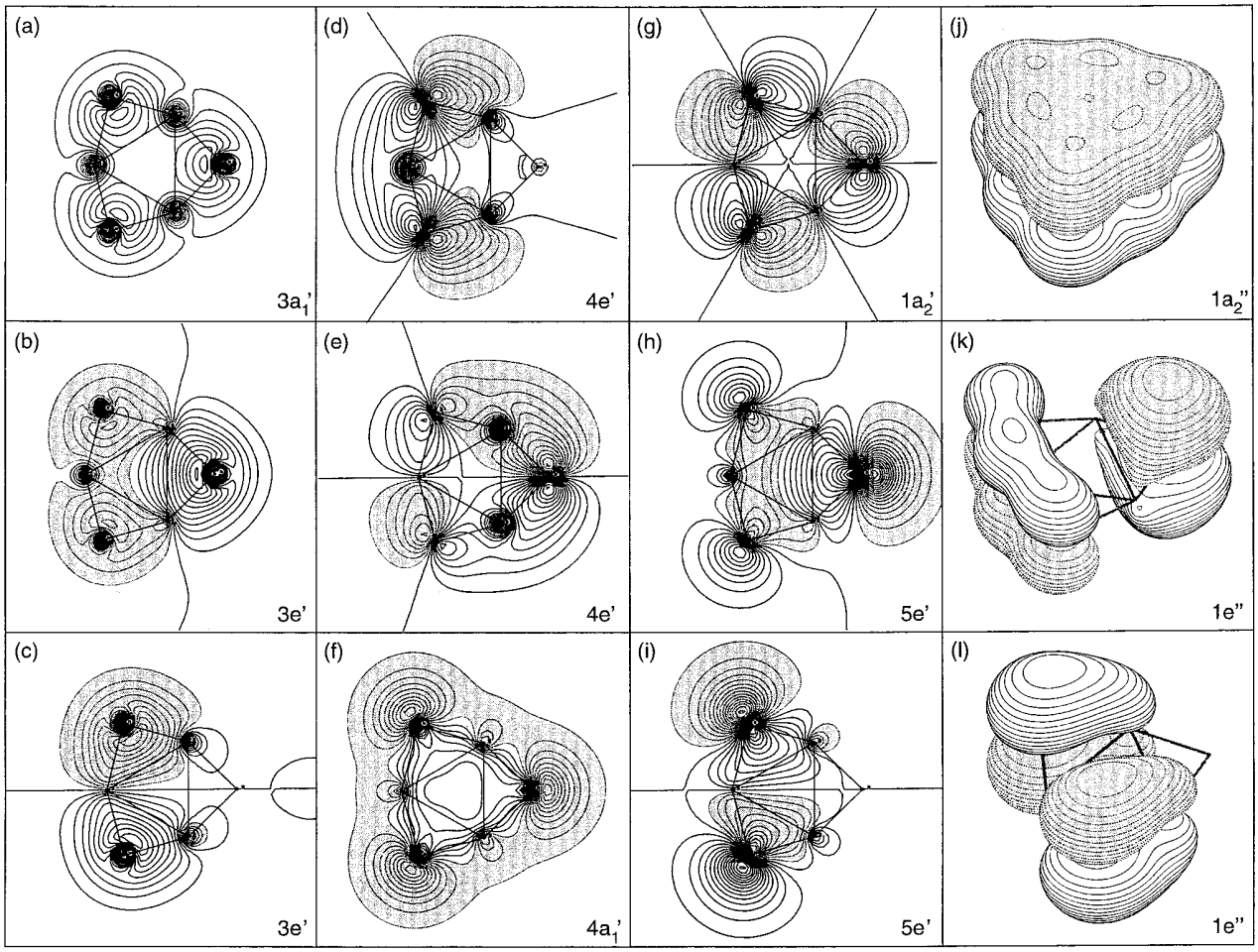

Figure 4. Valence occupied molecular orbitals of B_3N_3 corresponding to (or assimilated to) electron levels (a−c) of N_{2s} character and Σ symmetry; (d−f) $B_{2s} + N_{2p}$ character and Σ symmetry; (g−i) $B_{2p} + N_{2p}$ and Σ symmetry, and (j−l) $B_{2s} + N_{2p}$ character and Π symmetry. The orbitals of Σ symmetry are drawn using two-dimensional contour plots in the plane of the B_3N_3 ring, whereas orbitals of Π symmetry are displayed as three-dimensional plots.

TABLE 7: Detailed Analysis of the Lowest Unoccupied Molecular Orbital of the B_nN_n Rings Considered in This Study[a]

species	orbitals	$\%B_{2s}$	$\%B_{3s}$	$\%N_{2s}$	$\%N_{3s}$	$\%B_{2p}$	$\%B_{3p}$	$\%N_{2p}$	N_{3p}
B_3N_3	$5a_1'(\Sigma)$	**10**	**28**	8	14	**35**	1	3	0.8
B_4N_4	$5a_{1g}(\Sigma)$	**8**	**30**	6	28	**22**	2	3	0.6
B_5N_5	$5a_1'(\Sigma)$	0.06	**55**	2	**38**	0.005	0.09	3	2

[a] Percentages of N_{2s}, N_{2p}, B_{2s}, B_{2p}, N_{3s}, N_{3p}, B_{3s}, or B_{3p} atomic contributions. Character of the LUMO is evaluated from its LCAO coefficients (cc-pVDZ results).

boron sp^2 orbital character, with substantial B_{3s} contributions, and partial bonding character between the boron atoms. On the other hand, the very peculiar nodal structure of the LUMO ($5a_1'$) orbital of B_5N_5 (Figures 5c,f) indicates that this ring has become large enough to possibly bind and confine an additional electron within its internal cavity and along the main rotation axis, with some quantum tunneling from one side of the ring to the other through a small energy barrier. Both at the HF/cc-pVDZ and HF/aug-cc-pVDZ levels, the shape (Figures 5b,e) and intermediate LCAO content (Tables 7, 8) of the LUMO ($5a_{1g}$) of B_4N_4 foretell the transition observed with the LUMO of B_5N_5 (Figures 5c,f). These striking variations in the topology and composition of the LUMO obviously relate to a severe destabilization of the outward boron sp^2 orbitals from B_3N_3 to B_5N_5, as the θ_{NBN} bond angles approach 180°. In view of its diffuse character, the LUMO of B_5N_5 (and to a lesser extent B_4N_4) indicates a considerable Rydberg s-state character for the binding state of an additional electron. Unsurprisingly, therefore, the LCAO description of this state requires, at the HF/cc-pVDZ level, a very substantial proportion of B_{3s} atomic contributions (Table 7), and portends a particularly strong basis set dependence for the largest B_nN_n rings. Indeed, at the aug-cc-pVDZ level, the LUMO of the B_4N_4 and B_5N_5 clusters decomposes mostly into B_{4s} and N_{4s} atomic functions (Table 8). Relatedly, examination of the LUMO obtained from a HF/aug-cc-pVDZ calculation shows that inclusion of diffuse functions on the N and B atoms via the augmented cc-pVDZ basis results in a stronger delocalization of the LUMO of B_5N_5 within the ring cavity and along the main rotation axis (Figure 5f), at the expense of the outward boron sp^2 orbitals. Partial delocalization of the LUMO along the main rotation axis is also observed, to a much lesser extent, for B_4N_4 (Figure 5e), although in this case an additional electron becomes clearly excluded from the ring cavity, despite the inclusion of diffuse functions. On the other hand, the shape of the LUMO remains practically unchanged for B_3N_3 (compare Figure 5d to Figure 5a).

OVGF results for electron affinities (Tables 1−3) directly follow the destabilization of the lowest unoccupied lone-pair boron orbitals with increasing system size. Examination of the OVGF vertical affinity values for B_3N_3 (Table 1) indicates that its anion will be stable by at least 0.81 eV against electron loss, whereas a negative electron affinity (−0.66 eV) is obtained at

TABLE 8: Detailed Analysis of the Lowest Unoccupied Molecular Orbital of the B_nN_n Rings Considered in This Study (aug-cc-pVDZ results)

species	orbitals	$\%B_{2s}$	$\%B_{3s}$	$\%N_{2s}$	$\%N_{3s}$	$\%B_{2p}$	$\%N_{2p}$	$\%B_{3p}$	$\%N_{3p}$	$\%B_{4s}$	$\%N_{4s}$	$\%B_{4p}$	$\%N_{4p}$
B_3N_3	$5a_1'(\Sigma)$	5	7	3	2	9	1	0.1	0.002	**34**	**32**	6	1
B_4N_4	$5a_{1g}(\Sigma)$	0.02	0.03	0.01	2	0.1	0	0.01	0.03	**45**	**40**	7	1
B_5N_5	$5a_1'(\Sigma)$	0.02	2	0.4	2	0	0.08	0.2	0.03	**46**	**42**	4	2

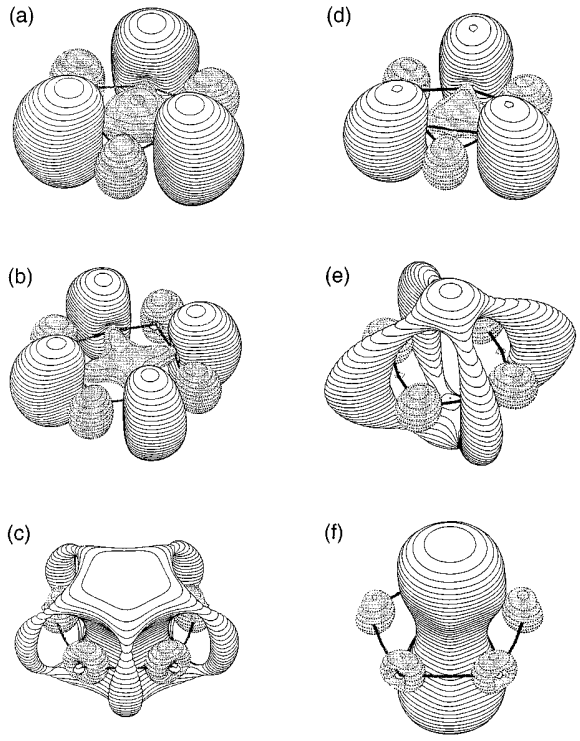

Figure 5. Lowest unoccupied molecular orbital of (a) B_3N_3: $5a_1'$ (b) B_4N_4: $4a_{1g}$, and (c) B_5N_5: $5a_1'$ at the HF/cc-pVDZ level, and (d,e,f; successively) at the HF/aug-cc-pVDZ level.

the HF level. On the other hand, a negative vertical electron affinity is obtained at both theoretical levels for B_4N_4 (Table 2) and B_5N_5 (Table 3). In view of their rather poor basis set contention and the opening of the band gap with increasing size, and since geometry relaxations are not accounted for, our OVGF results are, however, still insufficient to decide whether $B_4N_4^-$, $B_5N_5^-$, and larger $B_nN_n^-$ anions will be stable or decaying (i.e., short-lived and resonant) species.

The only quantitative trend that can be safely reported pertains to the role played by electron correlation and relaxation, which are found to result in a systematic increase, by 1.1−1.3 eV, of the vertical electron affinities, in comparison with the HF values. From the ionization energies and electron affinities obtained at the OVGF/aug-cc-pVDZ level, one can also infer a quasiparticle (i.e., OVGF) band gap of 11.98 eV for B_3N_3, 10.21 eV for B_4N_4, and 10.78 eV for B_5N_5.

4. Conclusions and Outlook for the Future

The electronic structure of B_nN_n ($n = 3-5$) clusters must be analyzed in terms of inner-valence levels of leading N_{2s} character, and outer-valence levels of mixed $B_{2s} + B_{2p} + N_{2p}$ character. According to this partition, our 1p-GF/ADC(3) calculations of one-electron binding and shake-up energies in these clusters indicate that the orbital picture of ionization is mostly valid for the $B_{2s} + B_{2p} + N_{2p}$ levels, whereas it completely breaks down at the level of the N_{2s} bands. Specific signatures for ring topologies involving ***n*** equivalent sharp B−N−B and dull N−B−N vertices can therefore be found in the outer-valence ionization bands of B_nN_n compounds.

HF data point out an opening of the fundamental band gap of B_nN_n clusters with increasing system size. This is clearly the outcome of a destabilization of the outward in-plane boron sp^2 orbitals which intimately relate to the LUMO of the smallest rings, as the N−B−N bridges approach linearity. Correspondingly, the onset of shake-up contamination is found to saturate at 15.6 eV for B_3N_3, 15.9 eV for B_4N_4, and 18.2 eV for B_5N_5. A comparison of the OVGF data obtained using the cc-pVDZ and augmented cc-pVDZ basis sets indicates that the former is largely sufficient to provide accurate one-hole ionization energies. By extrapolation of previous works on C_nH_{2n+2} compounds with similar band gaps,[38b] an extension of the 1p-GF/ADC(3) calculations to larger basis set would certainly lead to a redistribution of the spectral intensity of the innermost satellites to, e.g., shake-up transitions involving diffuse Rydberg states, but without significantly modifying the onset of shake-up contamination and the shape of the spectral bands.

Despite the breakdown of the orbital picture of ionization in the N_{2s} bands and the nonuniform influence of electronic relaxation and correlation on the outer-valence $B_{2s} + N_{2p}$ and $N_{2p} + B_{2p}$ bands, ionization spectra could be experimentally used to probe the orbital multiplicities and the details of the electronic structure of B_nN_n rings, and provide a definite proof for the existence of such structures in plasma conditions. The main (one-hole) ionization bands provide in particular specific signatures for ring topologies based on ***n*** equivalent vertices. For the investigated B_nN_n cluster species, multiplicity distribution can also be guessed from the overal symmetry of the N_{2s} bands. In addition, the latter can serve to follow a reduction of the curvature of N−B−N bridges with increasing system size, which has been found to strongly limit the spreading of N_{2s} lines.

Unlike ionization energies and the related pole strengths, the results obtained for vertical electron affinities show a very pronounced basis set dependence. Despite this difficulty, the calculations unequivocally indicate that the $B_3N_3^-$ anion is intrinsically stable, by at least 0.8 eV, against electron loss. On the other hand, the vertical electron affinities of B_4N_4 and B_5N_5 are negative but too small in absolute value to enable any definite conclusion. For these and larger boron−nitrogen clusters, detailed and accurate investigations of their adiabatic electron affinities, potential energy surfaces, and scattering potentials are required in order to evaluate the stability or decaying rate of $B_nN_n^-$ anions. Particularly large basis sets will obviously be required to describe reliably the binding and tunneling state of an additional electron along the main rotation axis and within the cavity of B_5N_5 and larger B_nN_n rings.

Acknowledgment. M.S.D. thanks the "Fonds voor Wetenschappelijk Onderzoek van Vlaanderen", the Flemish Science Foundation, for his Research Leader position at the Limburgs Universitair Centrum. M.G.G. acknowledges financial support from the "Bijzonder Onderzoeksfonds" (BOF) of the Limburgs Universitair Centrum.

References and Notes

(1) (a) *Gmelins Handbook of Inorganic Chemistry*, 8th ed.; Boron compounds, 3rd supplement, Vol. 3; Springer-Verlag: Berlin, 1988. (b) Paine, R. T.; Narula, C. K. *Chem. Rev.* **1990**, *90*, 73.

(2) Demazeau, G. *Diamond Relat. Mater.* **1995**, *4*, 284.
(3) Komatsu, S.; Yarbrough, W.; Moriyoshi, Y. *J. Appl. Phys.* **1997**, *81*, 7798 and references therein.
(4) *ZFI Mitteilungen*, nr. 134: *Beiträge zur Clusterforschung*, Akademie der Wissenschaften der DDR, September, 1987.
(5) Xia, X.; Jelski, D. A.; Bowser, J. R.; George, T. F. *J. Am. Chem. Soc.* **1992**, *114*, 6493.
(6) La Placa, S. J.; Roland, P. A.; Wynne, J. J. *Chem. Phys. Lett.* **1992**, *190*, 163.
(7) Jensen, F.; Toflund, H. *Chem. Phys. Lett.* **1993**, *201*, 89.
(8) Martin, J. M. L.; François, J.-P.; Gijbels, R. *J. Chem. Phys.* **1989**, *90*, 6469.
(9) Martin, J. M. L.; Lee, T. J.; Scuseria, G. E.; Taylor, P. R. *J. Chem. Phys.* **1992**, *97*, 6549.
(10) Slanina, Z.; Martin, J. M. L.; François, J.-P.; Gijbels, R. *Chem. Phys. Lett.* **1993**, *201*, 54.
(11) Andrews, L.; Hassandazeh, P.; Burkholder, T. R.; Martin, J. M. L. *J. Chem. Phys.* **1993**, *948*, 922.
(12) Martin, J. M. L.; Taylor, P. R.; François, J.-P.; Gijbels, R. *Chem. Phys. Lett.* **1994**, *222*, 517.
(13) Martin, J. M. L.; El-Yazal, J.; François, J.-P.; Gijbels, R. *Mol. Phys.* **1995**, *85*, 527.
(14) Peterson, K. A. *J. Chem. Phys.* **1995**, *102*, 262.
(15) Hassandazeh, P.; Andrews, L. *J. Phys. Chem.* **1992**, *96*, 9177.
(16) Knight, L. B., Jr.; Hill, D. W.; Kirk, T. J.; Arrington, C. A. *J. Phys. Chem.* **1992**, *96*, 555.
(17) Martin, J. M. L.; El-Yazal, J.; François, J. P. *Chem. Phys. Lett.* **1996**, *248*, 95.
(18) Sutjianto, A.; Pandey, R.; Recio, J. M. *Int. J. Quantum Chem.* **1994**, *52*, 199.
(19) Martin, J. M. L.; El-Yazal, J.; François, J.-P.; Gijbels, R. *Chem. Phys. Lett.* **1995**, *232*, 289.
(20) Cederbaum, L. S.; Domcke, W. *Adv. Chem. Phys.* **1977**, *36*, 205.
(21) Cederbaum, L. S.; Schirmer, J.; Domcke, W.; von Niessen, W. *Adv. Chem. Phys.* **1986**, *65*, 115.
(22) (a) Raghavachari, K.; Binkley, J. S. *J. Chem. Phys.* **1987**, *87*, 2191. (b) Martin, J. M. L.; El-Yazal, J.; François, J.-P. *Chem. Phys. Lett.* **1995**, *242*, 570. (c) Martin, J. M. L.; El-Yazal, J.; François, J.-P. *Chem. Phys. Lett.* **1996**, *252*, 9. (d) Giuffreda, M. G.; Deleuze, M. S.; François, J.-P. *J. Phys. Chem. A* **1999**, *103*, 5137.
(23) Ortiz, J. V.; Zakrzewski, V. G. *J. Chem. Phys.* **1994**, *100*, 6614.
(24) Deleuze, M. S.; Giuffreda, M. G.; François, J.-P.; Cederbaum, L. S. *J. Chem. Phys.* **1999**, *111*, 5851.
(25) Deleuze, M. S.; Giuffreda, M. G.; François, J.-P.; Cederbaum, L. S. *J. Chem. Phys.*, in press.
(26) Schirmer, J.; Cederbaum, L. S.; Walter, O. *Phys. Rev. A.* **1983**, *28*, 1237.
(27) Schirmer, J.; Angonoa, G. *J. Chem. Phys.* **1989**, *91*, 1754.
(28) Cederbaum, L. S. *J. Phys. B: Atom. Mol. Phys.* **1975**, *8*, 290.
(29) Ortiz, J. V.; Zakrzewski, V. G.; Dolgounircheva, O. One-Electron Pictures of Electronic Structures: Propagator Calculations of Photoelectron Spectra of Aromatic Molecules. In *Conceptual Perspectives in Quantum Chemistry*; Calais, J. L., Kryachko, E., Eds.; Kluwer Academic: Dordrecht, 1997; p 465.
(30) Dunning, T. H., Jr. *J. Chem. Phys.* **1989**, *90*, 1007.
(31) Martin J. M. L.; El-Yazal, J.; François, J.-P. *Mol. Phys.* **1995**, *86*, 1437.
(32) (a) Raghavachari, K.; Trucks, G. W.; Head-Gordon, M.; Pople, J. A. *Chem. Phys. Lett.* **1989**, *157*, 479. (b) Hample, C.; Peterson, K.; Werner, H. J. *Chem. Phys. Lett.* **1992**, *190*, 1. (c) Lee, J. T.; Scuseria, E. G. Achieving Chemical Accuracy with Coupled-Cluster Theory. In *Quantum Mechanical Electronic Structure Calculations with Chemical Accuracy*; Langhoff, S. R., Ed.; Kluwer: Dordrecht, 1995.
(33) Deleuze, M. S.; Delhalle, J.; Pickup, B. T.; Calais, J.-L. *Phys. Rev. B* **1992**, *46*, 15668. (b) Deleuze, M. S.; Delhalle, J.; Pickup, B. T.; Calais, J.-L. *Adv. Quantum Chem.* **1995**, *26*, 35.
(34) Schirmer, J.; Cederbaum, L. S. *J. Phys. B* **1978**, *11*, 1889.
(35) Weikert, H.-G.; Meyer, H.-D.; Cederbaum, L. S.; Tarantelli, F. *J. Chem. Phys.* **1996**, *104*, 7122.
(36) (a) Schirmer, J. *Phys. Rev. A* **1991**, *43*, 4647. (b) Mertins, F.; Schirmer, J. *Phys. Rev. A* **1996**, *53*, 2140.
(37) Deleuze, M. S.; Scheller, M. K.; Cederbaum, L. S. *J. Chem. Phys.* **1995**, *103*, 3578.
(38) (a) Deleuze, M. S.; Cederbaum, L. S. *Phys. Rev. B* **1996**, *53*, 13326. (b) Deleuze, M. S.; Cederbaum, L. S. *J. Chem. Phys.* **1996**, *105*, 7583. (c) Deleuze, M. S.; Cederbaum, L. S. *Int. J. Quantum Chem.* **1997**, *63*, 465. (d) Pang, W. N.; Gao, J. F.; Ruan, C. J.; Shang, R. C.; Trofimov, A. B.; Deleuze, M. S., submitted.
(39) Zobeley, J.; Cederbaum, L. S.; Tarantelli, F. *J. Chem. Phys.* **1998**, *108*, 9737.
(40) Deleuze, M. S.; Cederbaum, L. S. *Adv. Quantum Chem.* **1999**, *35*, 77.
(41) Golod, A.; Deleuze, M. S.; Cederbaum, L. S. *J. Chem. Phys.* **1999**, *110*, 6014.
(42) Schmidt, M. W.; Baldridge, K. K.; Boatz, J. A.; Jensen, J. H.; Koseki, S.; Gordon, M. S.; Nguyen, K. A.; Windus, T. L.; Elbert, S. T. *QCPE Bull.* **1990**, *10*, 52.
(43) Frisch, M. J.; Trucks, G. W.; Schlegel, H. B.; Scuseria, G. E.; Robb, M. A.; Cheeseman, J. R.; Zakrzewski, V. G.; Montgomery, J. A.; Stratmann, R. E.; Burant, J. C.; Dapprich, S.; Millam, J. M.; Daniels, A. D.; Kudin, K. N.; Strain, M. C.; Farkas, O.; Tomasi, V.; Barone, M.; Cossi, R.; Cammi, B.; Mennucci, C.; Pomelli, C.; Adamo, C.; Clifford, S.; Ochterski, J.; Petersson, G. A.; Ayala, P. Y.; Cui, Q.; Morokuma, K.; Malick, D. K.; Rabuck, A. D.; Raghavachari, K.; Foresman, J. B.; Cioslowski, J.; Ortiz, J. V.; Stefanov, B. B.; Liu, G.; Liashenko, A.; Piskorz, P.; Komaromi, I.; Gomperts, R.; Martin, R. L.; Fox, D. J.; Keith, T.; Al-Laham, M. A.; Peng, C. Y.; Nanayakkara, A.; Gonsalez, C.; Challacombe, M.; Gill, P. M. W.; Johnson, B. G.; Chen, W.; Wong, M. W.; Andres, J. L.; Head-Gordon, M.; Replogle, E. S.; and Pople, J. A. *Gaussian 98* (Revision A.1). Gaussian Inc.: Pittsburgh, PA, 1998.
(44) Kendall, R. A.; Dunning, T. H., Jr. *J. Chem. Phys.* **1992**, *96*, 6796.
(45) Int[X] denotes the largest integer contained within the real number X (e.g., Int[1.5] = 1).
(46) Trinastic, N. *Chemical graph theory*; C.R.C. Press: Boca Raton, FL, 1983; Vol. I, Chapter 6.